

Upper limits on the branching ratios

$$\tau \rightarrow \mu\gamma \text{ and } \tau \rightarrow e\gamma$$

DELPHI Collaboration

Abstract

The DELPHI collaboration has searched for lepton flavour violating decays $\tau \rightarrow \mu\gamma$ and $\tau \rightarrow e\gamma$ using a data sample of about 70 pb^{-1} of integrated luminosity corresponding to 81 000 produced $\tau^+\tau^-$ events. No candidates were found for either of the two modes. This yields branching ratio upper limits of $B(\tau \rightarrow e\gamma) < 1.1 \times 10^{-4}$ and $B(\tau \rightarrow \mu\gamma) < 6.2 \times 10^{-5}$ at 90% confidence level.

(To be submitted to Physics Letters B)

P.Abreu²¹, W.Adam⁵⁰, T.Adye³⁷, E.Agasi³¹, I.Ajinenko⁴², R.Aleksan³⁹, G.D.Alekseev¹⁶, P.P.Allport²², S.Almehed²⁴, S.J.Alvsvaag⁴, U.Amaldi⁹, S.Amato⁴⁷, A.Andreazza²⁸, M.L.Andrieux¹⁴, P.Antilogus²⁵, W-D.Apel¹⁷, Y.Arnoud³⁹, B.Åsman⁴⁴, J-E.Augustin¹⁹, A.Augustinus³¹, P.Baillon⁹, P.Bambade¹⁹, F.Barao²¹, R.Barate¹⁴, G.Barbiellini⁴⁶, D.Y.Bardin¹⁶, G.J.Barker³⁵, A.Baroncelli⁴⁰, O.Barring²⁴, J.A.Barrio²⁶, W.Bartl⁵⁰, M.J.Bates³⁷, M.Battaglia¹⁵, M.Baubillier²³, J.Baudot³⁹, K-H.Becks⁵², M.Begalli⁶, P.Beilliere⁸, Yu.Belokopytov⁹, A.C.Benvenuti⁵, M.Berggren⁴⁷, D.Bertrand², F.Bianchi⁴⁵, M.Bigi⁴⁵, M.S.Bilenky¹⁶, P.Billoir²³, D.Bloch¹⁰, M.Blume⁵², S.Blyth³⁵, V.Bocci³⁸, T.Bolognese³⁹, M.Bonesini²⁸, W.Bonivento²⁸, P.S.L.Booth²², G.Borisov⁴², C.Bosio⁴⁰, S.Bosworth³⁵, O.Botner⁴⁸, E.Boudinov⁴², B.Bouquet¹⁹, C.Bourdarios⁹, T.J.V.Bowcock²², M.Bozzo¹³, P.Branchini⁴⁰, K.D.Brand³⁶, T.Brenke⁵², R.A.Brenner¹⁵, C.Bricman², L.Brillault²³, R.C.A.Brown⁹, P.Bruckman¹⁸, J-M.Brunet⁸, L.Bugge³³, T.Buran³³, T.Burgsmueller⁵², P.Buschmann⁵², A.Buys⁹, M.Caccia²⁸, M.Calvi²⁸, A.J.Camacho Rozas⁴¹, T.Camporesi⁹, V.Canale³⁸, M.Canepa¹³, K.Cankocak⁴⁴, F.Cao², F.Carena⁹, P.Carrilho⁴⁷, L.Carroll²², C.Caso¹³, M.V.Castillo Gimenez⁴⁹, A.Cattai⁹, F.R.Cavallo⁵, L.Cerrito³⁸, V.Chabaud⁹, M.Chapkin⁴², Ph.Charpentier⁹, L.Chaussard²⁵, J.Chauveau²³, P.Checchia³⁶, G.A.Chelkov¹⁶, R.Chierici⁴⁵, P.Chliapnikov⁴², P.Chochula⁷, V.Chorowicz⁹, V.Cindro⁴³, P.Collins⁹, J.L.Contreras¹⁹, R.Contri¹³, E.Cortina⁴⁹, G.Cosme¹⁹, F.Cossutti⁴⁶, H.B.Crawley¹, D.Crennell³⁷, G.Crosetti¹³, J.Cuevas Maestro³⁴, S.Czellar¹⁵, E.Dahl-Jensen²⁹, J.Dahm⁵², B.Dalmagne¹⁹, M.Dam³³, G.Damgaard²⁹, A.Daum¹⁷, P.D.Dauncey³⁷, M.Davenport⁹, W.Da Silva²³, C.Defoix⁸, G.Della Ricca⁴⁶, P.Delpierre²⁷, N.Demaria³⁵, A.De Angelis⁹, H.De Boeck², W.De Boer¹⁷, S.De Brabandere², C.De Clercq², C.De La Vaissiere²³, B.De Lotto⁴⁶, A.De Min²⁸, L.De Paula⁴⁷, C.De Saint-Jean³⁹, H.Dijkstra⁹, L.Di Ciaccio³⁸, F.Djama¹⁰, J.Dolbeau⁸, M.Donszelmann⁹, K.Doroba⁵¹, M.Dracos¹⁰, J.Drees⁵², K.-A.Drees⁵², M.Dris³², Y.Dufour⁸, F.Dupont¹⁴, D.Edsall¹, R.Ehret¹⁷, G.Eigen⁴, T.Ekelof⁴⁸, G.Ekspung⁴⁴, M.Elsing⁵², J-P.Engel¹⁰, N.Ershaidat²³, B.Erzen⁴³, M.Espirito Santo²¹, E.Falk²⁴, D.Fassouliotis³², M.Feindt⁹, A.Ferrer⁴⁹, T.A.Filippas³², A.Firestone¹, P.-A.Fischer¹⁰, H.Foeth⁹, E.Fokitis³², F.Fontanelli¹³, F.Formenti⁹, B.Franek³⁷, P.Frenkiel⁸, D.C.Fries¹⁷, A.G.Frodesen⁴, R.Fruhvirth⁵⁰, F.Fulda-Quenzer¹⁹, J.Fuster⁴⁹, A.Galloni²², D.Gamba⁴⁵, M.Gandelman⁶, C.Garcia⁴⁹, J.Garcia⁴¹, C.Gaspar⁹, U.Gasparini³⁶, Ph.Gavillet⁹, E.N.Gazizadeh³², D.Gele¹⁰, J-P.Gerber¹⁰, M.Gibbs²², R.Gokhale⁵¹, B.Golob⁴³, G.Gopal³⁷, L.Gorn¹, M.Gorski⁵¹, Yu.Gouz⁴², V.Gracco¹³, E.Graziani⁴⁰, G.Grosdidier¹⁹, P.Gunnarsson⁴⁴, M.Gunther⁴⁸, J.Guy³⁷, U.Haeding¹⁷, F.Hahn⁹, M.Hahn¹⁷, S.Hahn⁵², Z.Hajduk¹⁸, A.Hallgren⁴⁸, K.Hamacher⁵², W.Hao³¹, F.J.Harris³⁵, V.Hedberg²⁴, R.Henriques²¹, J.J.Hernandez⁴⁹, P.Herquet², H.Herr⁹, T.L.Hessing⁹, E.Higon⁴⁹, H.J.Hilke⁹, T.S.Hill¹, S-O.Holmgren⁴⁴, P.J.Holt³⁵, D.Holthuizen³¹, M.Houlden²², J.Hrubec⁵⁰, K.Huet², K.Hultqvist⁴⁴, P.Ioannou³, J.N.Jackson²², R.Jacobsson⁴⁴, P.Jalocha¹⁸, R.Janik⁷, G.Jarlskog²⁴, P.Jarry³⁹, B.Jean-Marie¹⁹, E.K.Johansson⁴⁴, L.Jonsson²⁴, P.Jonsson²⁴, C.Joram⁹, P.Juillot¹⁰, M.Kaiser¹⁷, F.Kapusta²³, M.Karlsson⁴⁴, E.Karvelas¹¹, S.Katsanevas³, E.C.Katsoufis³², R.Keranen¹⁵, B.A.Khomenko¹⁶, N.N.Khovanski¹⁶, B.King²², N.J.Kjaer²⁹, H.Klein⁹, A.Klovning⁴, P.Kluit³¹, J.H.Koehne¹⁷, B.Koene³¹, P.Kokkinias¹¹, M.Koratzinos⁹, V.Kostioukhine⁴², C.Kourkoulis³, O.Kouznetsov¹³, P.-H.Kramer⁵², M.Kramer⁵⁰, C.Kreuter¹⁷, J.Krolikowski⁵¹, I.Kronkvist²⁴, Z.Krumstein¹⁶, W.Krupinski¹⁸, P.Kubinec⁷, W.Kucewicz¹⁸, K.Kurvinen¹⁵, C.Lacasta⁴⁹, I.Laktineh²⁵, S.Lamblot²³, J.W.Lamsa¹, L.Lanceri⁴⁶, D.W.Lane¹, P.Langefeld⁵², V.Lapin⁴², I.Last²², J-P.Laugier³⁹, R.Lauhakangas¹⁵, F.Ledroit¹⁴, V.Lefebvre², C.K.Legan¹, R.Leitner³⁰, Y.Lemoigne³⁹, J.Lemonne², G.Lenzen⁵², V.Lepeltier¹⁹, T.Lesiak³⁶, D.Liko⁵⁰, R.Lindner⁵², A.Lipniacka¹⁹, I.Lippi³⁶, B.Loerstad²⁴, M.Lokajicek¹², J.G.Loken³⁵, J.M.Lopez⁴¹, A.Lopez-Fernandez⁹, M.A.Lopez Aguera⁴¹, D.Loukas¹¹, P.Lutz³⁹, L.Lyons³⁵, J.MacNaughton⁵⁰, G.Maehlum¹⁷, A.Maio²¹, V.Malychev¹⁶, F.Mandi⁵⁰, J.Marco⁴¹, B.Marechal⁴⁷, M.Margoni³⁶, J.-C.Marin⁹, C.Mariotti⁴⁰, A.Markou¹¹, T.Maron⁵², C.Martinez-Rivero⁴¹, F.Martinez-Vidal⁴⁹, S.Marti i Garcia⁴⁹, K.Marvik⁴, F.Matorras⁴¹, C.Matteuzzi²⁸, G.Matthiae³⁸, M.Mazzucato³⁶, M.Mc Cubbin⁹, R.Mc Kay¹, R.Mc Nulty²², J.Medbo⁴⁸, C.Meroni²⁸, W.T.Meyer¹, M.Michelotto³⁶, E.Migliore⁴⁵, L.Mirabito²⁵, W.A.Mitaroff⁵⁰, U.Mjoernmark²⁴, T.Moa⁴⁴, R.Moeller²⁹, K.Moenig⁹, M.R.Monge¹³, P.Morettini¹³, H.Mueller¹⁷, L.M.Mundim⁶, W.J.Murray³⁷, B.Muryn¹⁸, G.Myatt³⁵, F.Naraghi¹⁴, F.L.Navarria⁵, S.Navas⁴⁹, P.Negri²⁸, S.Nemecek¹², W.Neumann⁵², N.Neumeister⁵⁰, R.Nicolaidou³, B.S.Nielsen²⁹, M.Nieuwenhuizen³¹, V.Nikolaenko¹⁰, P.Niss⁴⁴, A.Nomerotski³⁶, A.Normand³⁵, W.Oberschulte-Beckmann¹⁷, V.Obraztsov⁴², A.G.Olshevski¹⁶, R.Orava¹⁵, K.Osterberg¹⁵, A.Ouraou³⁹, P.Paganini¹⁹, M.Paganoni⁹, P.Pages¹⁰, H.Palka¹⁸, Th.D.Papadopoulou³², L.Pape⁹, C.Parkes³⁵, F.Parodi¹³, A.Passeri⁴⁰, M.Pegoraro³⁶, L.Peralta²¹, H.Pernegger⁵⁰, M.Pernicka⁵⁰, A.Perrotta⁵, C.Petridou⁴⁶, A.Petrolini¹³, H.T.Phillips³⁷, G.Piana¹³, F.Pierre³⁹, M.Pimenta²¹, M.Pindo²⁸, S.Plaszczynski¹⁹, O.Podobrin¹⁷, M.E.Pol⁶, G.Polok¹⁸, P.Poropat⁴⁶, V.Pozdniakov¹⁶, M.Prest⁴⁶, P.Privitera³⁸, N.Pukhaeva¹⁶, A.Pullia²⁸, D.Radojicic³⁵, S.Ragazzi²⁸, H.Rahmani³², J.Rames¹², P.N.Ratoff²⁰, A.L.Read³³, M.Reale⁵², P.Rebecchi¹⁹, N.G.Redaeli²⁸, M.Regler⁵⁰, D.Reid⁹, P.B.Renton³⁵, L.K.Resvanis³, F.Richard¹⁹, J.Richardson²², J.Ridky¹², G.Rinaudo⁴⁵, I.Ripp³⁹, A.Romero⁴⁵, I.Roncagliolo¹³, P.Ronchese³⁶, L.Roos¹⁴, E.I.Rosenberg¹, E.Rosso⁹, P.Roudeau¹⁹, T.Rovelli⁵, W.Ruckstuhl³¹, V.Ruhlmann-Kleider³⁹, A.Ruiz⁴¹, K.Rybicki¹⁸, H.Saarikko¹⁵, Y.Sacquin³⁹, A.Sadovsky¹⁶, G.Sajot¹⁴, J.Salt⁴⁹, J.Sanchez²⁶, M.Sannino¹³, H.Schneider¹⁷, M.A.E.Schyns⁵², G.Sciolla⁴⁵, F.Scuri⁴⁶, Y.Sedykh¹⁶, A.M.Segar³⁵, A.Seitz¹⁷, R.Sekulin³⁷, R.C.Shellard⁶, I.Siccama³¹, P.Siegrist³⁹, S.Simonetti³⁹, F.Simonetto³⁶, A.N.Sisakian¹⁶, B.Sitar⁷, T.B.Skaali³³, G.Smadja²⁵, N.Smirnov⁴², O.Smirnova¹⁶, G.R.Smith³⁷, R.Sosnowski⁵¹, D.Souza-Santos⁶, T.Spaso²¹, E.Spiriti⁴⁰, P.Sponholz⁵², S.Squarcia¹³, C.Stanescu⁴⁰, S.Stapnes³³, I.Stavitski³⁶, K.Stepaniak⁵¹, F.Stichelbaut⁹, A.Stocchi¹⁹, J.Strauss⁵⁰, R.Strub¹⁰, B.Stugu⁴, M.Szczekowski⁵¹, M.Szeptycka⁵¹, T.Tabarelli²⁸, J.P.Tavernet²³, O.Tchikilev⁴², A.Tilquin²⁷,

J. Timmermans³¹, L.G. Tkatchev¹⁶, T. Todorov¹⁰, D.Z. Toet³¹, A. Tomaradze², B. Tome²¹, L. Tortora⁴⁰, G. Transtomer²⁴, D. Treille⁹, W. Trischuk⁹, G. Tristram⁸, A. Trombini¹⁹, C. Troncon²⁸, A. Tsirou⁹, M-L. Turluer³⁹, I.A. Tyapkin¹⁶, M. Tyndel³⁷, S. Tzamarias²², B. Ueberschaer⁵², O. Ullaland⁹, V. Uvarov⁴², G. Valenti⁵, E. Vallazza⁹, C. Vander Velde², G.W. Van Apeldoorn³¹, P. Van Dam³¹, W.K. Van Doninck², J. Van Eldik³¹, N. Vassilopoulos³⁵, G. Vegni²⁸, L. Ventura³⁶, W. Venus³⁷, F. Verbeure², M. Verlato³⁶, L.S. Vertogradov¹⁶, D. Vilanova³⁹, P. Vincent²⁵, L. Vitale⁴⁶, E. Vlasov⁴², A.S. Vodopyanov¹⁶, V. Vrba¹², H. Wahlen⁵², C. Walck⁴⁴, M. Weierstall⁵², P. Weilhammer⁹, A.M. Wetherell⁹, D. Wicke⁵², J.H. Wickens², M. Wielers¹⁷, G.R. Wilkinson³⁵, W.S.C. Williams³⁵, M. Winter¹⁰, M. Witek⁹, K. Woschnagg⁴⁸, K. Yip³⁵, O. Yushchenko⁴², F. Zach²⁵, C. Zacharitou²⁴, A. Zaitsev⁴², A. Zalewska¹⁸, P. Zalewski⁵¹, D. Zavrtnik⁴³, E. Zevgolatakos¹¹, N.I. Zimin¹⁶, M. Zito³⁹, D. Zontar⁴³, R. Zuberi³⁵, G.C. Zucchelli⁴⁴, G. Zumerle³⁶

¹Ames Laboratory and Department of Physics, Iowa State University, Ames IA 50011, USA

²Physics Department, Univ. Instelling Antwerpen, Universiteitsplein 1, B-2610 Wilrijk, Belgium and IHEE, ULB-VUB, Pleinlaan 2, B-1050 Brussels, Belgium

and Faculté des Sciences, Univ. de l'Etat Mons, Av. Maistriau 19, B-7000 Mons, Belgium

³Physics Laboratory, University of Athens, Solonos Str. 104, GR-10680 Athens, Greece

⁴Department of Physics, University of Bergen, Allégaten 55, N-5007 Bergen, Norway

⁵Dipartimento di Fisica, Università di Bologna and INFN, Via Irnerio 46, I-40126 Bologna, Italy

⁶Centro Brasileiro de Pesquisas Físicas, rua Xavier Sigaud 150, RJ-22290 Rio de Janeiro, Brazil and Depto. de Física, Pont. Univ. Católica, C.P. 38071 RJ-22453 Rio de Janeiro, Brazil

and Inst. de Física, Univ. Estadual do Rio de Janeiro, rua São Francisco Xavier 524, Rio de Janeiro, Brazil

⁷Comenius University, Faculty of Mathematics and Physics, Mlynska Dolina, SK-84215 Bratislava, Slovakia

⁸Collège de France, Lab. de Physique Corpusculaire, IN2P3-CNRS, F-75231 Paris Cedex 05, France

⁹CERN, CH-1211 Geneva 23, Switzerland

¹⁰Centre de Recherche Nucléaire, IN2P3 - CNRS/ULP - BP20, F-67037 Strasbourg Cedex, France

¹¹Institute of Nuclear Physics, N.C.S.R. Demokritos, P.O. Box 60228, GR-15310 Athens, Greece

¹²FZU, Inst. of Physics of the C.A.S. High Energy Physics Division, Na Slovance 2, 180 40, Praha 8, Czech Republic

¹³Dipartimento di Fisica, Università di Genova and INFN, Via Dodecaneso 33, I-16146 Genova, Italy

¹⁴Institut des Sciences Nucléaires, IN2P3-CNRS, Université de Grenoble 1, F-38026 Grenoble Cedex, France

¹⁵Research Institute for High Energy Physics, SEFT, P.O. Box 9, FIN-00014 Helsinki, Finland

¹⁶Joint Institute for Nuclear Research, Dubna, Head Post Office, P.O. Box 79, 101 000 Moscow, Russian Federation

¹⁷Institut für Experimentelle Kernphysik, Universität Karlsruhe, Postfach 6980, D-76128 Karlsruhe, Germany

¹⁸High Energy Physics Laboratory, Institute of Nuclear Physics, Ul. Kawioru 26a, PL-30055 Krakow 30, Poland

¹⁹Université de Paris-Sud, Lab. de l'Accélérateur Linéaire, IN2P3-CNRS, Bât. 200, F-91405 Orsay Cedex, France

²⁰School of Physics and Materials, University of Lancaster, Lancaster LA1 4YB, UK

²¹LIP, IST, FCUL - Av. Elias Garcia, 14-1º, P-1000 Lisboa Codex, Portugal

²²Department of Physics, University of Liverpool, P.O. Box 147, Liverpool L69 3BX, UK

²³LPNHE, IN2P3-CNRS, Universités Paris VI et VII, Tour 33 (RdC), 4 place Jussieu, F-75252 Paris Cedex 05, France

²⁴Department of Physics, University of Lund, Sölvegatan 14, S-22363 Lund, Sweden

²⁵Université Claude Bernard de Lyon, IPNL, IN2P3-CNRS, F-69622 Villeurbanne Cedex, France

²⁶Universidad Complutense, Avda. Complutense s/n, E-28040 Madrid, Spain

²⁷Univ. d'Aix - Marseille II - CPP, IN2P3-CNRS, F-13288 Marseille Cedex 09, France

²⁸Dipartimento di Fisica, Università di Milano and INFN, Via Celoria 16, I-20133 Milan, Italy

²⁹Niels Bohr Institute, Blegdamsvej 17, DK-2100 Copenhagen 0, Denmark

³⁰NC, Nuclear Centre of MFF, Charles University, Areal MFF, V Holesovickach 2, 180 00, Praha 8, Czech Republic

³¹NIKHEF-H, Postbus 41882, NL-1009 DB Amsterdam, The Netherlands

³²National Technical University, Physics Department, Zografou Campus, GR-15773 Athens, Greece

³³Physics Department, University of Oslo, Blindern, N-1000 Oslo 3, Norway

³⁴Dpto. Física, Univ. Oviedo, C/P. Pérez Casas, S/N-33006 Oviedo, Spain

³⁵Department of Physics, University of Oxford, Keble Road, Oxford OX1 3RH, UK

³⁶Dipartimento di Fisica, Università di Padova and INFN, Via Marzolo 8, I-35131 Padua, Italy

³⁷Rutherford Appleton Laboratory, Chilton, Didcot OX11 0QX, UK

³⁸Dipartimento di Fisica, Università di Roma II and INFN, Tor Vergata, I-00173 Rome, Italy

³⁹Centre d'Etudes de Saclay, DSM/DAPNIA, F-91191 Gif-sur-Yvette Cedex, France

⁴⁰Istituto Superiore di Sanità, Ist. Naz. di Fisica Nucl. (INFN), Viale Regina Elena 299, I-00161 Rome, Italy

⁴¹C.E.A.F.M., C.S.I.C. - Univ. Cantabria, Avda. los Castros, S/N-39006 Santander, Spain, (CICYT-AEN93-0832)

⁴²Inst. for High Energy Physics, Serpukov P.O. Box 35, Protvino, (Moscow Region), Russian Federation

⁴³J. Stefan Institute and Department of Physics, University of Ljubljana, Jamova 39, SI-61000 Ljubljana, Slovenia

⁴⁴Fysikum, Stockholm University, Box 6730, S-113 85 Stockholm, Sweden

⁴⁵Dipartimento di Fisica Sperimentale, Università di Torino and INFN, Via P. Giuria 1, I-10125 Turin, Italy

⁴⁶Dipartimento di Fisica, Università di Trieste and INFN, Via A. Valerio 2, I-34127 Trieste, Italy

and Istituto di Fisica, Università di Udine, I-33100 Udine, Italy

⁴⁷Univ. Federal do Rio de Janeiro, C.P. 68528 Cidade Univ., Ilha do Fundão BR-21945-970 Rio de Janeiro, Brazil

⁴⁸Department of Radiation Sciences, University of Uppsala, P.O. Box 535, S-751 21 Uppsala, Sweden

⁴⁹IFIC, Valencia-CSIC, and D.F.A.M.N., U. de Valencia, Avda. Dr. Moliner 50, E-46100 Burjassot (Valencia), Spain

⁵⁰Institut für Hochenergiephysik, Österr. Akad. d. Wissensch., Nikolsdorfergasse 18, A-1050 Vienna, Austria

⁵¹Inst. Nuclear Studies and University of Warsaw, Ul. Hoza 69, PL-00681 Warsaw, Poland

⁵²Fachbereich Physik, University of Wuppertal, Postfach 100 127, D-42097 Wuppertal 1, Germany

1 Introduction

Lepton flavour violation has never been observed in nature. In the Standard Model, however, there is no fundamental reason why lepton flavour should be conserved. Instead, conservation of lepton flavour is assured by assuming zero mass for neutrinos. For non-zero neutrino masses and mixing between neutrino flavours the Standard Model predicts very low, but non-zero, rates for decays such as $\tau \rightarrow \mu\gamma$ and $\tau \rightarrow e\gamma$. Several extensions to the Standard Model give room for larger rates. These include models with additional heavy neutrinos [1], and models of supersymmetric grand unification, where the branching ratio $B(\tau \rightarrow \mu\gamma)$ is expected to exceed $B(\mu \rightarrow e\gamma)$ by five orders of magnitude [2]. Models which are symmetric with respect to left- and right-handed leptons can accommodate rates which are within reach given current experimental possibilities [3].

At LEP τ leptons are produced through the reaction $e^+e^- \rightarrow Z^0 \rightarrow \tau^+\tau^-$ at a centre of mass energy on or close to the Z^0 mass. The τ pairs are cleanly separated from $q\bar{q}$ events through the low multiplicity of the decay products, and from electron and muon pairs through the energy carried away by the undetected neutrinos. In the following a search for the two decay modes $\tau \rightarrow \mu\gamma$ and $\tau \rightarrow e\gamma$ is presented. The main signatures of these decay modes are that all the energy of the initial τ should be seen, and that the invariant mass of the observed decay products should equal the τ mass. The data sample used was collected by the DELPHI experiment from 1990 through 1993 and corresponds to an integrated luminosity of about 70 pb^{-1} .

2 Detector description

DELPHI is a general purpose detector with a magnetic field of 1.2 Tesla provided by a large superconducting solenoid. The principal detector components used in this investigation were the tracking devices for track and momentum reconstruction, the electromagnetic calorimeters for electron and photon identification, and the hadron calorimeters and muon chambers for muon identification. The main tracking device was the Time Projection Chamber (TPC) which is a large drift chamber extending over radial distances R from 35 to 111 cm. The tracking was supplemented by the Vertex Detector (VD), the Inner Detector (ID) and the Outer Detector (OD) to reconstruct charged particle tracks at large angles to the beam axis. For particles emerging at smaller angles, the forward drift chambers (FCA and FCB) supplemented the TPC for track reconstruction. The electromagnetic calorimetry consisted of an array of lead glass blocks (FEMC) in the polar angular regions $0.804 < |\cos \theta| < 0.985$ and of the High density Projection Chamber (HPC) for $|\cos \theta| < 0.73$ where θ is the polar angle measured with respect to the e^- beam direction. The HPC was radially segmented into 9 layers, and was built up of a total of 144 modules. The hadron calorimeter (HCAL) was radially segmented into 4 layers and covered 98% of the solid angle. For muon detection, chambers were placed between the third and the fourth HCAL layer and outside the fourth layer, covering nearly the same solid angle. A detailed description of the DELPHI detector can be found in [4].

3 Preselection of $\tau^+\tau^-$ pairs

Starting with events with a charged track multiplicity, N_{ch} , of $2 \leq N_{ch} \leq 6$, the charged particle tracks were divided into hemispheres by a plane perpendicular to the event thrust axis. The highest momentum particle in at least one of the hemispheres should have a

polar angle satisfying $|\cos \theta| < 0.94$. The main criteria for preselecting $\tau^+\tau^-$ pairs from Z^0 decays took advantage of the fact that in a standard τ decay a substantial part of the energy is carried away by the neutrino(s), or by the γ in the modes which were sought in this analysis. In order to preserve efficiency even when the neutral particles in one hemisphere carry little energy, the neutral or missing energy in both hemispheres was taken into account simultaneously. The variable $P_{rad} = \sqrt{P_1^2 + P_2^2}$, where P_1 and P_2 are the momenta of the leading particles in hemisphere 1 and 2 respectively, was particularly useful. Similarly, to remove e^+e^- pairs, a variable $E_{rad} = \sqrt{E_1^2 + E_2^2}$ was defined using the electromagnetic energies associated to the leading charged particle. Another characteristic of the τ decay products observed in the detector is that they, contrary to e^+e^- and $\mu^+\mu^-$ pairs from Z^0 decays, are expected to be acollinear, where acollinearity is defined as 180° minus the angle between the resultant momentum vectors from each hemisphere.

Events in which at least one particle had $|\cos \theta| < 0.73$ should satisfy the conditions $P_{rad} < P_{beam}$ and $E_{rad} < E_{beam}$, where P_{beam} and E_{beam} denote the beam momentum and energy. Furthermore a minimum acollinearity of 0.5° was imposed for events with only one charged particle per hemisphere. For events where all particles had $|\cos \theta| > 0.73$ these cuts were tightened by requiring $P_{rad} < 0.9 \times P_{beam}$ and $E_{rad} < 0.9 \times E_{beam}$, and the acollinearity for events with two charged particles was required to exceed 2° .

To reduce the background from events stemming from $\gamma\gamma$ collisions and cosmic rays the following requirements were imposed for all events: A minimum visible energy of $0.2 \times E_{beam}$ was demanded; a minimum transverse momentum for the event of $0.4 \text{ GeV}/c$ was imposed; the distance of closest approach of the leading tracks to the nominal interaction point was required to be less than 1.5 cm in the plane transverse to the beam and less than 4.5 cm in the z coordinate (along the beam).

4 Particle identification and background rejection

As a first step, individual τ decay candidates with more than one charged particle were rejected. A minimum momentum of $2 \text{ GeV}/c$ on the single particle was also required.

The electron identification was restricted to charged particles in the region $|\cos \theta| < 0.71$. This is well within the angular coverage of the HPC and electrons are thus expected to deposit all their energy in the HPC. Requiring the ratio $E_{HPC}/E_{track} > 0.5$ selected electrons with high efficiency. Here E_{HPC} is the energy deposit in the HPC and E_{track} is the particle energy inferred from the momentum measurement. Furthermore, the leakage of shower energy into the hadron calorimeter should not exceed 1 GeV .

Muons could be identified both from the muon chamber response and from the response of the hadronic calorimeter. Only particles with an energy deposit in the electromagnetic calorimeters (HPC and FEMC) of less than 1.5 GeV were considered. The hit information in the muon chambers was used by performing a fit of the extrapolated track to the hits in the chambers, retaining candidates passing the fit. The response from the HCAL was required to be compatible with a minimum ionising particle. After normalising the HCAL energy deposit to the equivalent deposit at normal incidence, the compatibility was ensured by requiring a total energy deposit in the HCAL larger than 1 GeV , including more than 200 MeV in the outermost layer, and an average energy deposit per layer less than 3 GeV . If the reconstructed polar angle of the muon candidate was such that $|\cos \theta| < 0.71$ it was accepted as a muon if it passed either the muon chamber analysis

or the HCAL analysis. In events where the leading particle in both hemispheres had $|\cos\theta| \geq 0.71$, muon candidates should satisfy both requirements.

For each hemisphere, the most energetic cluster found in the electromagnetic calorimeters and not associated to a charged particle track was retained as a possible γ candidate provided it had an energy above 1 GeV. If the neutral was found in the HPC, a deposition of energy of at least 200 MeV in at least two consecutive layers was required. To suppress photons from bremsstrahlung in the detector, the reconstructed shower axis was required to agree to within 10° with the direction expected for a photon coming from the interaction point.

4.1 Background suppression

Important sources of background were e^+e^- and $\mu^+\mu^-$ pairs, with one or more extra photons present. Most of these were removed by requiring that the total energy in the hemisphere opposite to candidate events should be less than 80% of the beam energy. All events with a muon candidate in both hemispheres were removed from the search if both reconstructed particles satisfied $|\cos\theta| > 0.73$. For events with at least one particle in the range $|\cos\theta| < 0.73$ and a muon candidate in both hemispheres, P_{rad} was required to be less than $0.8 \times P_{beam}$. In addition, special care had to be taken of events close to boundaries between detector modules. Events where one of the two leading tracks projected back to within 1.5° of the boundary between TPC modules were thus rejected. If one of the two leading tracks projected in ϕ to within 1.0° of the border between two HPC modules, the E_{rad} requirement was tightened to $< 0.6 \times E_{beam}$. When the charged particle track opposite to an $e\gamma$ candidate pointed into this border region, the energy deposition in the hadron calorimeter was used to reject electrons. If the energy deposit in the first layer of the hadron calorimeter was larger than 3 GeV while no energy was deposited in the two outermost layers, the event was discarded; this suppressed the e^+e^- background further.

5 Simulation

Kinematically, $\tau \rightarrow \mu\gamma$ and $\tau \rightarrow e\gamma$ decays are almost identical to the mode $\tau \rightarrow \pi\nu_\tau$ at LEP energies. The $\pi\nu_\tau$ mode has an angular distribution of

$$W(\theta^*) = \frac{1}{2}(1 + P_\tau \cos\theta^*) \quad (1)$$

where P_τ is the τ polarisation and θ^* is the emission angle in the τ rest frame. The most general form for the modes sought can be written

$$W(\theta^*) = \frac{1}{2}(1 + AP_\tau \cos\theta^*) \quad (2)$$

with $-1 \leq A \leq 1$. $A = 1(-1)$ corresponds to only left-handed (right-handed) photon helicity in the decays.

A total of 6000 τ pair events were generated with an $e\gamma$ or $\mu\gamma$ final state in one hemisphere by using the KORALZ [5] event generator. The second τ in the event was required to decay into one of its standard modes in agreement with the known properties of the τ . In order to study systematic effects, half of the events were generated with $A = 1$ and the other half with $A = -1$. The events were tracked through the detector using a full simulation of the DELPHI detector, and subsequently reconstructed with

the same program as the real data. The simulated momentum and energy resolutions were cross checked by the use of e^+e^- and $\mu^+\mu^-$ pairs. Corrections to the HPC energy resolution found for electrons were also applied to photon candidates.

6 Selection of $e\gamma$ and $\mu\gamma$ candidate events

If the decays $\tau \rightarrow \mu\gamma$ and $\tau \rightarrow e\gamma$ did take place, all the initial energy of the decaying τ should have been seen in the detector. Furthermore, the invariant mass of the lepton photon system, $m_{l\gamma}$, should equal the τ mass. In the samples of simulated $\tau \rightarrow \mu\gamma$ and $\tau \rightarrow e\gamma$ decays some correlation is observed between energy and mass, and it was convenient to study the data using the variables defined by:

$$E' = (E_{l\gamma} - E_{beam}) \cos \alpha + (m_{l\gamma}c^2 - m_\tau c^2) \sin \alpha \quad (3)$$

and

$$m' = (m_{l\gamma}c^2 - m_\tau c^2) \cos \alpha - (E_{l\gamma} - E_{beam}) \sin \alpha, \quad (4)$$

For an appropriate choice of α , the distribution in m' can be made symmetric, while the E' distribution appears with a tail towards low values. The optimal value of the rotation angle α was determined to be $\alpha = 2.2^\circ$. This gave the highest signal efficiency, when defining a preliminary contour for the signal region. For simulated $\tau \rightarrow \mu\gamma$ events, the m' distribution had a standard deviation of .09 GeV, and the central part of the E' distribution had a standard deviation of 2.04 GeV. A signal region consisting of the area within the 2.5σ contour was defined. This requirement is formulated by defining a variable R given by the equation

$$R = \sqrt{\left(\frac{E'}{5.1\text{GeV}}\right)^2 + \left(\frac{m'}{0.23\text{GeV}}\right)^2} \quad (5)$$

which should be less than unity for candidate events. The corresponding $\tau \rightarrow e\gamma$ distributions had a similar width in m' , but the E' distribution had a much more pronounced tail. Since more background is expected in this channel, the signal region was not redefined to include more of this tail. Instead, the $\tau \rightarrow \mu\gamma$ contour was used to define the signal region also in the $\tau \rightarrow e\gamma$ search. Figures 1a) and b) show the reconstructed energy versus invariant mass for simulated events with the contour ellipse superimposed. In figures 2 and 3 the distributions of the variable R are displayed for the simulated signal events and for all the data. The distributions of R are shown for the events reconstructed, and for those events which remain after rejecting background as described in section 4.1.

After applying these requirements, no events remained with $R < 1$. Figures 1c) and 1d) display the reconstructed energy versus invariant mass for $e\gamma$ and $\mu\gamma$ candidates, after being subjected to the full analysis. Although the signal region contained no events, some background might be expected. The events close to the signal region might be of two kinds. Firstly, radiative e^+e^- and $\mu^+\mu^-$ pairs could still be present. These events would satisfy the energy conservation condition, but they have a continuous spectrum of invariant masses because of the continuous spectrum of the emission angle of the γ candidate with respect to the charged particle. However, from a sample of simulated e^+e^- and $\mu^+\mu^-$ events corresponding to about three times the statistics in the data, no events passed full analysis. The second important background consists of τ decays. These events can be leptonic τ decays with a radiated γ . $e\gamma$ candidates can also be formed from decays with one charged and one or more neutral pions. The reconstructed energies and

masses resulting from these backgrounds extend into the signal region. From a sample of simulated $\tau^+\tau^-$ pairs, the background levels expected were 0.6 ± 0.4 events for the $\tau \rightarrow e\gamma$ analysis and 0.3 ± 0.3 events for the $\tau \rightarrow \mu\gamma$ search.

7 Estimate of limits

The efficiency of the analysis was estimated from simulation and cross-checked by comparison with data. The efficiency of the electron and muon identification was cross-checked by verifying that the measured branching fractions of the decays $\tau \rightarrow \mu\nu\bar{\nu}$ and $\tau \rightarrow e\nu\bar{\nu}$ were consistent with the known values [6]. The systematic uncertainties on the charged particle identification efficiency has been estimated to be slightly below $\pm 2\%$, and $\pm 2\%$ was taken as a systematic uncertainty for this.

The photon identification efficiency was checked by the use of $\mu^+\mu^-\gamma$ events. Using the event generator DYMU3 [7] and full detector simulation, the number of reconstructed photons per event was compared to the corresponding number in the data after selecting events with a pair of muons. Energy dependence and dependence on the opening angle between the muon and the neutral cluster was studied. Good agreement between data and simulation was observed for opening angles appropriate for this analysis. To cross-check, τ decays with detected photons from π^0 decays were used. τ decays containing electron and muon candidates were removed, and the spectrum of the most energetic photon candidate was studied. A comparison between simulation and data did not show any energy dependent discrepancy, but an overall correction factor for the efficiency of photon detection calculated from simulation of 0.98 ± 0.02 was deduced. The linearity of the energy estimate of the photon candidates was checked by using kinematically constrained $e^+e^-\gamma$ and $\mu^+\mu^-\gamma$ events. A small overestimate of the reconstructed energies could not be excluded in the data. This did not affect the $e\gamma$ efficiency notably as such an overestimate would pull more of the tail into the signal region. However, such a shift would lead to a decrease of 2% in the $\mu\gamma$ efficiency and was included as a systematic uncertainty. Other systematic effects studied include those due to the unknown momentum distribution in the events searched for due to the unknown value of A in eq. (2). These studies were done on independent samples of simulated events, and the effects were found to be small compared to the uncertainty due to the simulated event statistics.

The efficiency with respect to the full solid angle was thus estimated at $(14.6 \pm 0.8)\%$ for the $e\gamma$ final state and $(24.5 \pm 1.2)\%$ for the $\mu\gamma$ final state. Using measured cross-sections [8] and estimates of the effective integrated luminosity, the number of τ decays within the full solid angle was estimated to be 162 000. Using the 90% confidence level lower limits of the efficiencies this leads to the following upper limits:

$$B(\tau \rightarrow e\gamma) < 1.1 \times 10^{-4}$$

$$B(\tau \rightarrow \mu\gamma) < 6.2 \times 10^{-5}$$

at 90% confidence level. The $\tau \rightarrow e\gamma$ result is comparable to the ARGUS result of $B(\tau \rightarrow e\gamma) < 1.2 \times 10^{-4}$ [9]. The result on $\tau \rightarrow \mu\gamma$ is however surpassed by $B(\tau \rightarrow \mu\gamma) < 4.2 \times 10^{-6}$ from CLEO [10] which is currently the most stringent limit on that decay mode.

Acknowledgements

We are greatly indebted to our technical collaborators and to the funding agencies for their support in building and operating the DELPHI detector, and to the members of the CERN-SL Division for the excellent performance of the LEP collider.

References

- [1] J.W.F. Valle, Prog. in Nucl. and Part. Physics **26** (1991) 91.
- [2] R. Barbieri and L.J. Hall, Phys. Lett. **B338** (1994) 212.
- [3] R. N. Mohapatra, Phys. Rev. **D46** (1992) 2990.
- [4] DELPHI Collaboration, P. Aarnio et al., Nucl. Instr. Meth. **A303** (1991) 233.
- [5] S. Jadach and Z. Was, Comp. Phys. Commun. **36** (1985) 191;
S. Jadach, B.F.L. Ward and Z. Was, Comp. Phys. Commun. **66** (1991) 276.
- [6] Particle Data Group, Phys. Rev. **D50** (1994) 1173.
- [7] J.E. Campagne and R. Zitoun, Zeit. Phys. **C43** (1989) 459; Proc. of the Brighton Workshop on Radiative Corrections, Sussex, July 1989.
- [8] DELPHI Collaboration, P. Abreu et al., Nucl. Phys. **B418** (1994) 403.
DELPHI Collaboration, P. Abreu et al., Zeit. Phys. **C55** (1992) 555.
- [9] ARGUS Collaboration, H. Albrecht et al., Zeit. Phys. **C55** (1992) 179.
- [10] CLEO Collaboration, A. Bean et al., Phys. Rev. Lett. **70** (1993) 138.

DELPHI

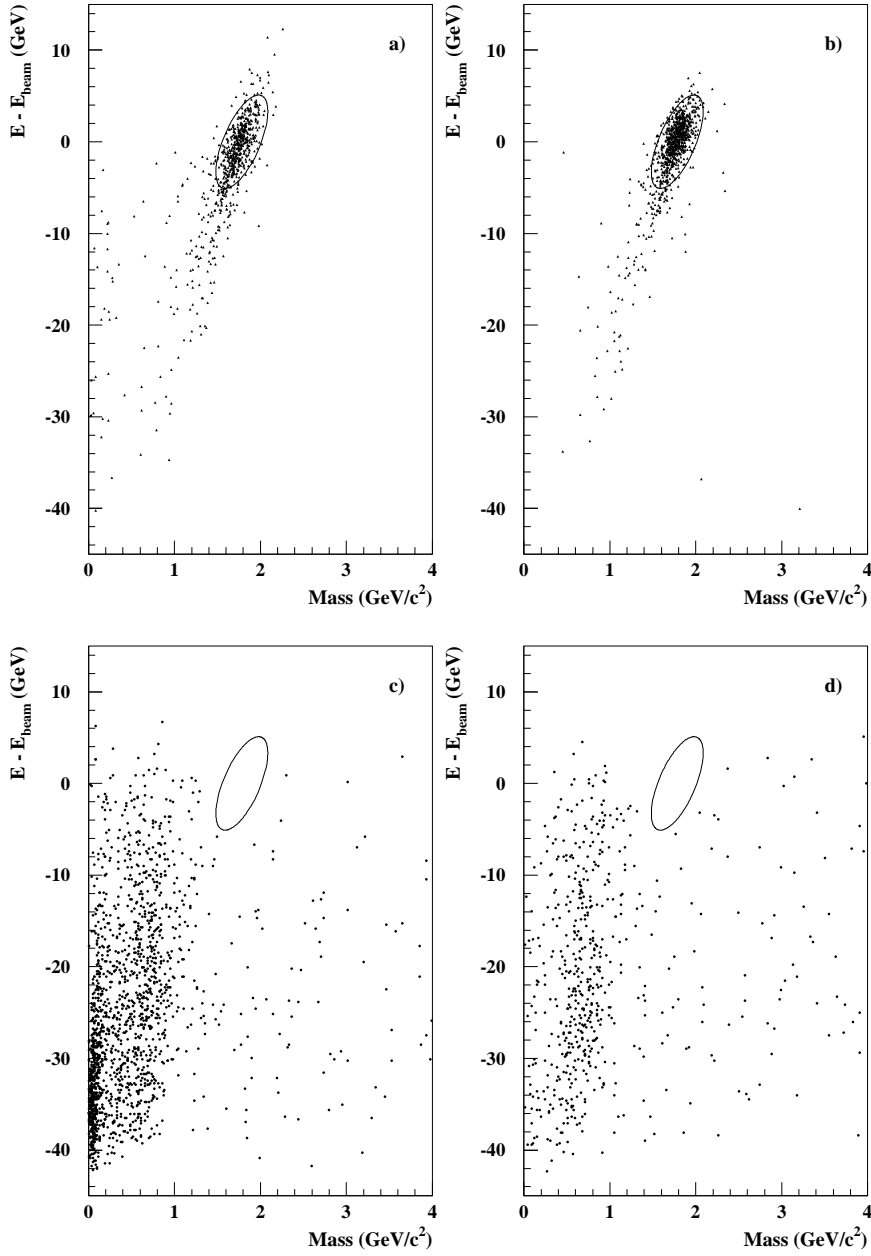


Figure 1: Reconstructed energy minus beam energy vs. invariant mass. a) Simulated $\tau \rightarrow e\gamma$ events, b) Simulated $\tau \rightarrow \mu\gamma$ events, c) $e\gamma$ candidates, d) $\mu\gamma$ candidates. The signal region was defined by the ellipse which is superimposed on the figures.

DELPHI

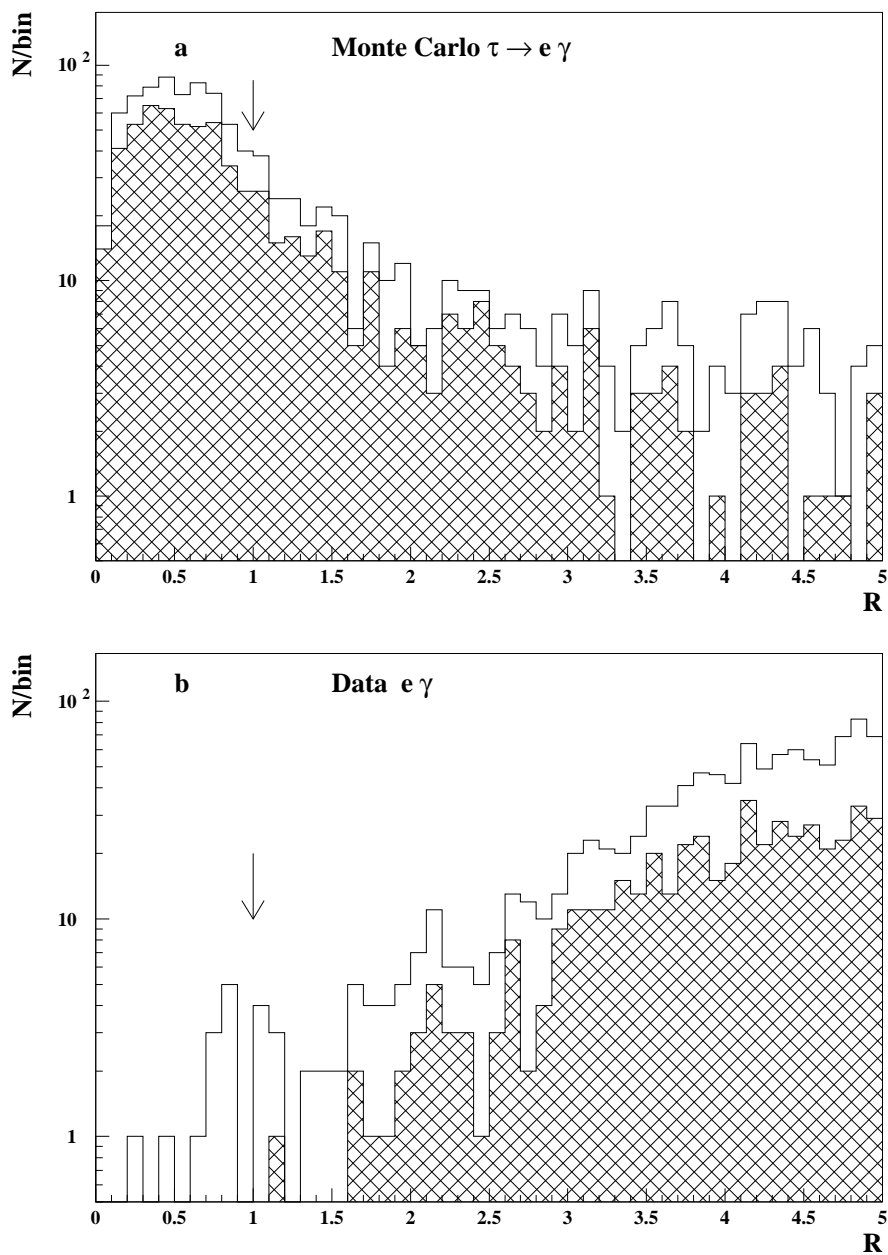


Figure 2: Distribution in the variable R for $\tau \rightarrow e\gamma$ candidates. a) Simulated events, b) data. Open histograms are before the background rejection described in section 4.1, hatched histograms are after these requirements. No events remain in the signal region, $R < 1$.

DELPHI

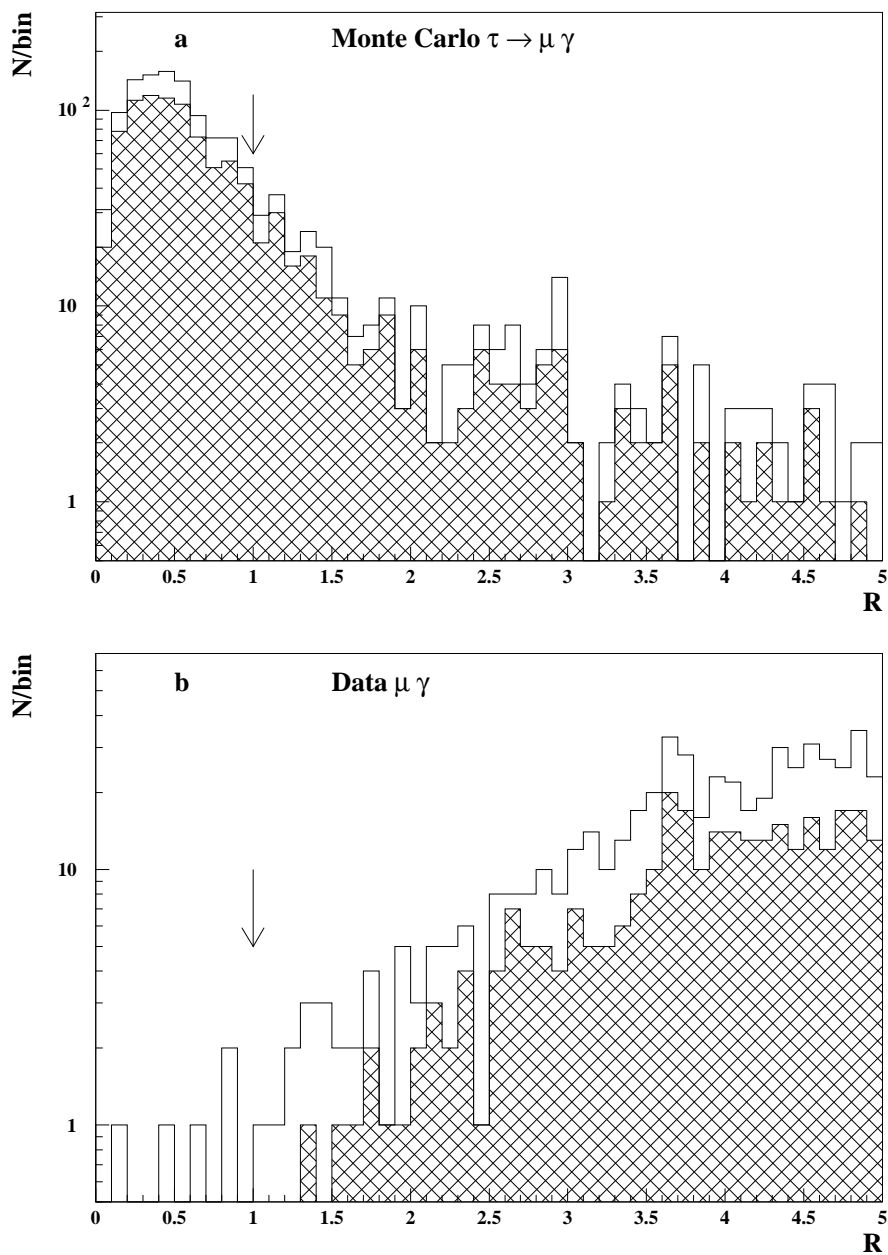


Figure 3: Distribution in the variable R for $\tau \rightarrow \mu \gamma$ candidates. a) Simulated events, b) data. Open histograms are before the background rejection described in section 4.1, hatched histograms are after these requirements. No events remain in the signal region, $R < 1$.